Microstructure of equilibrium fluid clusters in colloid-polymer suspensions

V. Gopalakrishnan and C. F. Zukoski*
Department of Chemical and Biomolecular Engineering, University of Illinois, Urbana, Illinois 61801, USA
(Received 19 July 2006; published 27 February 2007)

Several studies on colloidal depletion systems have reported the existence of a fluid phase consisting of clusters of particles above a critical polymer concentration that acts as a precursor regime to the gel phase at low colloid volume fractions ($\phi \leq 0.20$). The clusters are found to be stable against further aggregation suggesting that individual particles are localized within a cluster. However the clusters themselves behave as distinct entities in an equilibrium fluid phase. In this study, we probe the internal microstructure of the cluster entities by ultrasmall angle x-ray scattering (USAXS) techniques. These studies reveal that over the accessible length scales, the microstructure of the particle clusters are similar to that observed in dense space-spanning depletion gels. The origin of these clusters is unclear but the scattering patterns as they settle with time reveal that the percolation of the clusters to form space-spanning gels does not influence their internal microstructure. These observations lend support to the hypothesis that the formation of space-spanning depletion gels at a given volume fraction is driven by the percolation of the particle clusters. Settling experiments at $\phi=0.08$ also provide rough estimates of the cluster sizes that appear consistent with the observations from the USAXS experiments.

DOI: 10.1103/PhysRevE.75.021406 PACS number(s): 82.70.Dd

I. INTRODUCTION

As the strength of attraction between colloidal particles is increased, aggregation occurs. In dense suspensions this is often accompanied by the formation of a space-filling gel [1–7] in which particles undergo long-range diffusion in a sluggish manner if at all. The result is a material displaying the elastic properties of a soft solid. Under dilute conditions, aggregation is often accompanied by the formation of clusters. A great deal of work has gone into understanding the structure of clusters formed in systems where the strength of attraction at contact is essentially infinite such that particles within clusters cannot rearrange [8–11]. Under these conditions the clusters formed tend to have open, fractal structures. Because the clusters occupy a much larger volume than their constituent particles, in the absence of other forces, these systems can form gels at incredibly low particle volume fractions. There are, however, other types of microstructures that occur in aggregated and gelled suspensions. In particular, some systems form dense clusters. This can occur with the addition of polymer flocculants [12–14] and precipitation reactions [15–17]. With precipitation reactions, understanding dense-floc formation is complicated by the chemical reactions that accompany dense cluster formation.

Here we explore the properties of dense clusters formed by depletion attractions that are induced between hard-sphere particles when a nonadsorbing polymer is added. Colloidal depletion systems display liquid-liquid, liquid-liquid-crystal, liquid-crystal, and gel transitions depending on the particle and polymer concentrations and the ratio of the polymer radius of gyration, R_g, to particle radius, R. When $R_g/R < \sim 0.1$, for polymers in theta and good solvents, suspensions experiencing depletion attractions form gels above a critical polymer concentration. In dense suspensions, these are space filling. At lower volume fractions, the suspensions form gels that can display delayed sedimentation [18], and at lower volume fraction still, the suspensions form dense aggregated structures, that in the absence of gravity are reported to be stable [13] against further aggregation but in the presence of a density mismatch between the particles and the solvent, settle to form a dense sediment.

At low polymer and low particle concentrations, the suspension of individual particles is stable against any aggregation with the particles assuming the microstructure of a liquid of weakly attractive particles. Above a critical polymer concentration, the particles spontaneously assemble into clusters, defined in this study as the boundary between fluid and fluid-cluster phases. For our system consisting of particles of silica with surface-coated octadecyl hydrocarbon chains suspended in decalin, the density mismatch is such that the resulting clusters settle. As the particle concentrations are further raised space-filling gels are produced.

Gel formation is attributed to the presence of attractive bonds between particles that prevent long-range motion and keep particles localized. Naïve mode coupling theory (NMCT) [19] calculations that incorporate the impact of the suspension microstructure on particle dynamics have been successful in predicting the gel-phase boundary when compared to experiments on well characterized experimental systems. However, mode coupling approaches [19–23] are incapable of accounting for the development of dense clusters in which the particles are localized with respect to one another but which remain mobile as distinct units. Of key interest is an understanding of what sets the size of these clusters and if they retain their integrity as the particle volume fraction or strength of attraction increases.

One possibility for the mechanism controlling a stable cluster size [24] is that the particles experience long-range Coulombic repulsions that limit the size to which clusters can grow. As the charge on the particles increases, the cluster size decreases. This hypothesis is indeed supported by

*Author to whom correspondence should be addressed; Electronic address: czukoski@uiuc.edu

experimental observations [12,25–27] of stable clusters in conditions involving attractions in the presence of long-range repulsions. However, Lu *et al.* [13] recently obtained clusters in density matched conditions even after screening the long-range repulsions and these clusters were found to be stable for several days. Thus it appears that the fundamental origins of the cluster formation remain unsolved.

Here, we explore the internal microstructure of the dense clusters using ultrasmall angle x-ray scattering (USAXS) techniques on a well characterized experimental colloidal depletion system. This system enables us to probe length scales ranging from a particle diameter up to length scales that are nearly two orders in magnitude larger. Since there exists a density mismatch between the particles (octadecyl-coated silica) and the solvent (decalin), the clusters settle with time enabling us to track the evolution of the microstructure as the particles consolidate to form a space-spanning gel. By comparing the microstructures over time, we show that the internal microstructure of the clusters is identical to that observed in space-spanning dense depletion gels [28,29] at much higher particle volume fractions. This suggests that colloidal gelation in depletion systems is driven by the percolation of the clusters and not an internal restructuring of the clusters close to the gel boundary. From settling experiments, we obtain size estimates of the particle clusters that agree with our observations of the absence of a Guinier plateau at the lowest accessible wave vectors in the scattering experiments.

In Sec. II, we discuss the techniques for sample preparation and the different experimental procedures involved. Section III presents the various experimental results. The scattering data is analyzed using the Debye-Bueche model [30] for scattering from a "random two-phase" system in Sec. IV and comparisons are made with observations in the work of Shah *et al.* [29] and Ramakrishnan *et al.* [28] on dense depletion gels. In Sec. V, we present estimates for the size of the cluster from our settling experiments and show that the values are consistent with our observations from the scattering experiments. Finally, in Sec. VI, we present our conclusions.

II. MATERIALS AND METHODS

Silica particles are synthesized, as per the method of Stober *et al.* [31], by the base catalyzed hydrolysis of *tetra*-ethyl orthosilicate (purchased from the Sigma Aldrich company) in an ethanol medium. By using a predetermined recipe of concentrations of the ingredients, the desired seed size for the silica particles is achieved. The seed particles are then grown to their final size by employing the "double addition" technique of Bogush and Zukoski [32]. The final particle radius achieved was, $R=42.5$ nm which was confirmed by scanning electron microscopy (SEM) images, dynamic light scattering measurements and from ultrasmall angle x-ray scattering (USAXS) patterns. These particles are then surface-coated with octadecanol by the procedure recommended by van Helden *et al.* [33]. After the coating procedure, the particles are repeatedly (3–6 times) washed with chloroform and centrifuged to remove the unreacted octadecanol. The washed particles are then dried in a vacuum oven for 24 hours to eliminate all traces of the wash solvent. The hydrophobic coating of octadecyl chains enables the particles to be suspended in a number of organic solvents. In this study, decalin is used as the solvent medium.

Depletion attractions between the particles are induced by adding polystyrene polymer of molecular weight, $M_w = 18\,700$ gms/mol. As per the characterization results of Shah *et al.* [1], which show that decalin is a near-ideal solvent for polystyrene, the polymer has a radius of gyration, $R_g=3.6$ nm. The ratio of the polymer radius of gyration to the particle radius, $R_g/R=0.085$, sets the range of attraction between the particles. The polymer concentration, c, which sets the strength of the depletion attraction, is normalized to the characteristic polymer concentration for overlap, $c^*=4M_w/(3\pi N_A R_g^3)$ where N_A is the Avogadro number.

To get suspensions at a certain volume fraction, ϕ, and particular polymer concentration, c/c^*, we add requisite amounts of stock colloid suspension and polymer solution and make-up decalin. We have performed two sets of experiments, one in which we track the settling behavior of the suspensions in the fluid cluster phase and the second where we perform USAXS runs on these same settling samples. Below we describe the procedure for both sets of experiments.

A. Settling

Above the boundary between fluid and fluid-cluster phases, the suspension is composed of clusters that settle rapidly under the influence of gravity. The settling behavior of these suspensions was studied in glass capillary tubes with a diameter of 0.2 cm. Well-mixed suspensions were loaded carefully into the capillary tubes with glass syringes to a height of ~ 2 cm. The open end of the tubes was flame-sealed immediately and rapidly to avoid any solvent evaporation. The tube was then left undisturbed in a closed environment (defined as zero time) and the interface of the settling sediment, defined as its height, was observed as a function of elapsed time. The height measurements were made with a nonintrusive telescopic eye piece that was attached to a Vernier scale with an accuracy of 0.001 cm. Similar settling experiments were also performed on the same sample cells in which the USAXS runs were performed. As seen in the inset of Fig. 2, the initial settling velocities fall within the same window of values independent of the sample cell geometry.

B. Ultrasmall angle x-ray scattering (USAXS)

The side-bounce ultrasmall angle x-ray scattering (SB-USAXS) setup at the Advanced Photon Source (APS) at the Argonne National Laboratories, Illinois was employed for this study. The setup consists of two sets of channel-cut Si 111 crystals that define the x-ray beam and eliminate slit-smearing effects of the scattered intensity. This obviates the need for a desmearing routine of the extracted scattering data. An advantage of the setup is that the static structure factor, $S(q)$ from these experiments directly provides an accurate measure of the density correlations in the suspension over a large window of wave vectors, q, ranging from a

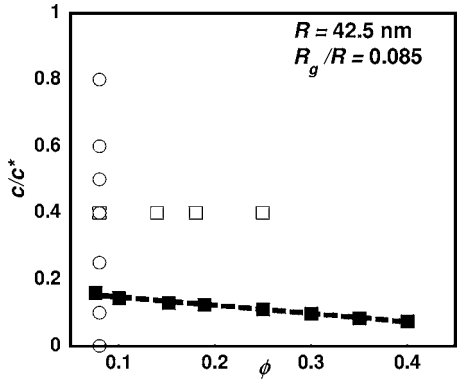

FIG. 1. Normalized polymer concentration, c/c^* as a function of colloid volume fraction, ϕ. The solid symbols are the experimentally determined gel boundary for a similar experimental system [35] at a near-equivalent $R_g/R=0.078$. At the lower volume fractions, i.e., $\phi<0.2-0.3$, the gel boundary is characterized by the formation of particle clusters that eventually sediment to the bottom of the vial. The open circles are samples at a constant. $\phi=0.08$ and different polymer concentrations. The open squares represent samples with a constant $c/c^*=0.4$ and different volume fractions.

$2qR\sim0.1$ up to the first peak in the structure factor, $2qR\sim7.5$ for our study.

USAXS experiments were performed in a custom-made aluminum sample cell where the sample is loaded between two Kapton polyimide films with a path length of 0.1 cm. The cell geometry is such that the sample facing the incident beam has a circular cross section with a diameter of ~1 cm. Prior to loading the sample, it is well mixed. Once loaded, the fluid sample composed of particle clusters begins to settle to the bottom of the cell with time. Immediately after loading the sample (i.e., after ~8 minutes), a 15 minute scattering run is carried out by scanning the center of the sample cell over the entire range of accessible wave vectors. As the sample settles, further scans are carried out at regular intervals. At these times, scans are performed at a distance of 0.3 cm below the center of the cell. This ensures that for all the scans we are indeed probing the microstructure in the consolidating sediment and not the supernatant. The time mentioned in all figures denotes the time elapsed after the sample was loaded into the cell. It should be noted that since the scans take ~15 minutes to complete, the scattering pattern reflects an averaged structure over the period of the scan (~15 minutes). However since this time frame is negligible compared to the time scale over which the sample settles, this does not influence our results.

III. EXPERIMENTAL RESULTS

Figure 1 displays the critical polymer concentrations for the crossover from the equilibrium fluid phase to the gel phase ($\phi>0.2$) or the fluid-cluster phase ($\phi<0.2$) at conditions similar to that employed in our study. This crossover is visually identified by the first observation of a turbid phase. In our study, for one set of experiments, the volume fraction was kept constant ($\phi=0.08$) and the polymer concentration was varied between $c/c^*=0-0.8$ (shown by the open circles in the figure). For the second set of experiments, the polymer concentration was kept constant ($c/c^*=0.4$) and the volume fraction was varied between $\phi=0.08-0.25$ (shown by the open squares in the figure). Most of our discussion will focus on the first set of experiments since the conclusions drawn from the second set of experiments are similar. Unless specified, the volume fraction values refer to the initial concentration of the individual particles at time, $t=0$.

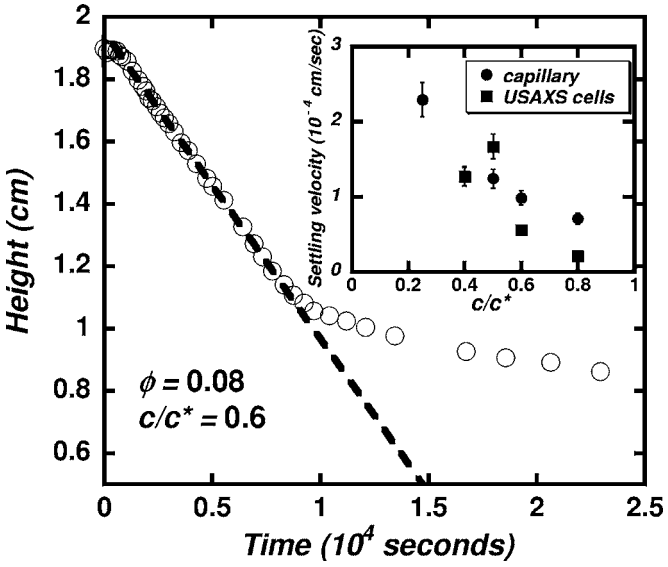

FIG. 2. Sediment height as a function of elapsed time. The open symbols are experimental points at $\phi=0.08$ and $c/c^*=0.6$. The settling profiles at the other polymer concentrations look similar. The dotted line is a linear fit to the initial settling regime. The inset is a figure of the initial settling velocity at $\phi=0.08$ over the range of explored polymer concentration. In addition to the measurements in 2 mm capillaries (circles), settling velocities were also measured in the sample cells (squares) in which the USAXS scattering experiments were performed.

No evidence of settling was observed for samples below the fluid-fluid-cluster phase boundary. However, above the phase boundary, suspensions settle slowly. Dynamic light scattering (DLS) experiments, performed at a normalized wave vector of $qR\sim1.2$ in a back-scattering geometry to minimize the path length through the sample and eliminate multiple scattering, reveal a complete decorrelation of the intensity autocorrelation function for the explored polymer concentrations. This indicates that above the phase boundary, the suspensions are not gelled. Figure 2 shows a plot of the settling height against time of the fluid-cluster suspension with $\phi=0.08$ and $c/c^*=0.6$. The interface between the turbid phase and the particle free phase is sharp and the height of this interface initially decreases linearly with time. At long times (not shown in the figure), the interface-height asymptotes to a constant value. The initial settling velocity is shown as a function of the polymer concentration for $\phi=0.08$ in the inset of Fig. 2. Here the measurements made in capillary tubes are compared against those made in USAXS sample cells. For both sets of measurements, we observe a decrease in the initial settling velocity with increasing polymer concentration.

We initially discuss the scattering profiles from the USAXS experiments. The inset plot of Fig. 3(a) shows the

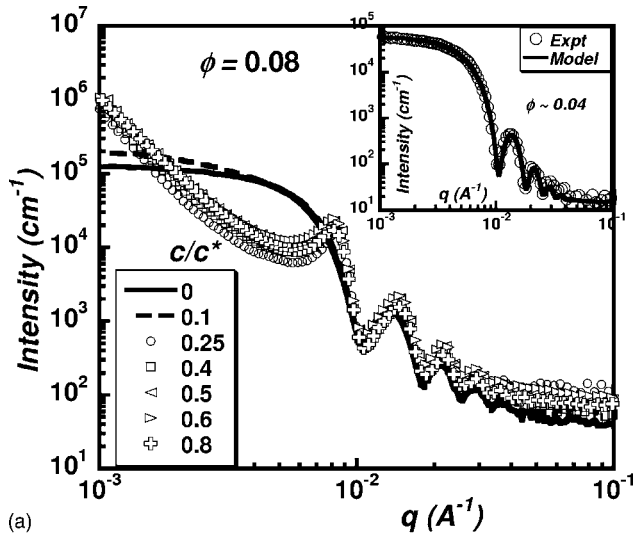

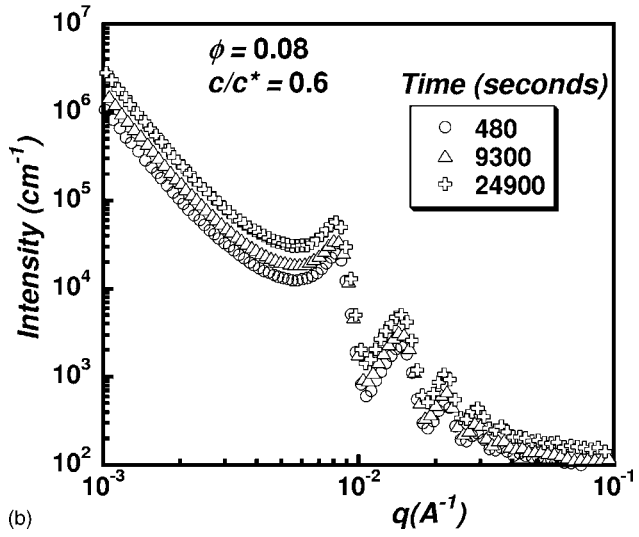

FIG. 3. (a) Scattering intensity as a function of the wave vector, q. The inset plot shows the scattering pattern for a very low volume fraction sample where we expect interparticle interference effects to be negligible. As a result, the scattering represents the form factor of the particle. The form-factor fit (solid line) for a sphere of radius, $R=42.5$ nm captures the experimental data. The main plot is for the various polymer concentrations at $\phi=0.08$. As seen in the figure, scattering from the $c/c^*=0$ and $c/c^*=0.1$ suspensions which are below the gel boundary (Fig. 1) show neither a low angle upturn nor a scattering peak at $q\sim0.0085$ A^{-1}. Above the boundary between fluid and fluid-cluster phases , all samples display scattering patterns with both these features that are signatures of depletion gels at much higher volume fractions [29,35]. (b) Scattering intensity as a function of the wave vector, q at different times after loading the sample. The qualitative features of the scattering profiles are retained with time. However the scattering pattern is shifted to higher intensities with increasing time. The above features are replicated for all the explored polymer concentrations.

scattered intensity against the wave vector from a sample with $\phi=0.04$ and no polymer. At this volume fraction, the scattered intensity is entirely dominated by the form factor of the particle. As seen, the form factor for spherical particles with a mean radius, $R=42.5$ nm, and standard deviation of 1.8 nm in the particle-size distribution is capable of capturing the experimental scattering data for the entire window of accessible wave vectors. The model employs a Gaussian particle size distribution weighted form factor to obtain a fit to the experimental data by the method of least squares.

The effect of polymer concentration on the scattering from a suspension at $\phi=0.08$ is given in Fig. 3(a). For the samples with $c/c^*=0$ and $c/c^*=0.1$, which are below the boundary between fluid and fluid-cluster phases, the scattering patterns are very similar to that obtained from hard sphere suspensions at similar volume fractions. However above the boundary between fluid and fluid-cluster phases, a completely different picture emerges. At the lowest wave vectors, the scattered intensity increases sharply above that for the samples below the phase boundary. At intermediate wave vectors, 0.002 A$^{-1}<q<0.007$ A^{-1}, the intensity is suppressed relative to that for the equilibrium fluid samples. An interesting feature is the appearance of a peak in the scattered intensity at $q\sim0.0085$ A^{-1}. The peak is similar to that obtained for hard sphere suspensions at volume fractions of $\phi>0.30-0.40$.

The evolution of the scattered intensity of the consolidating portion of the sample at $\phi=0.08$ and $c/c^*=0.6$ with time in Fig. 3(b) shows that the qualitative features of the scattering pattern are retained as time progresses. However, the curves are shifted upwards to higher intensities with increasing time. The scattered intensity, $I_{sc}(q)=(\phi/\phi_{ff})I_{ff}(q)S(q)$ where, ϕ_{ff} is the volume fraction of the suspension used to measure the form factor of the particles and $I_{ff}(q)$ is the angle-dependent scattering from this low volume fraction sample. Since the form factor of the particles [and hence $I_{ff}(q)$] and ϕ_{ff} are constant, the increase in the scattered intensity, $I_{sc}(q)$, would be attributed to either an increase in the volume fraction or an increase in the correlations of density fluctuations which are quantified by $S(q)$, i.e., $I_{sc}(q)\alpha\phi S(q)$. Therefore, $[I_{sc}(q)]_f/[I_{sc}(q)]_0=(\phi_f/\phi_0)[S(q)_f/S(q)_0]$ where the subscript "f" stands for the final scattering run and "0" stands for first scattering run. As time progresses, clusters of the particles consolidate at the base of the sample cell. Since we ensure that all scattering runs are performed on the consolidated part of the sample, we know that the volume fraction of the particles increases with time. As shown in the inset plot of Fig. 2, the settling velocities in both the capillary tubes and the USAXS sample cells are nearly identical. Hence, we can use the measurements of the settling heights in the capillary tubes to get an estimate of how the volume fraction of the particles increases in the sediment portion of the sample with time. Table I displays values for (ϕ_f/ϕ_0) [where $(\phi_f/\phi_0)=(H_0/H_f)$ and H is the sediment height] from the settling experiments in capillary tubes and the factor $[I_{sc}(q)]_f/[I_{sc}(q)]_0$ that is required to scale the scattered intensities of the first and last runs for a given sample onto a single curve.

As seen from Table I, the increase in the magnitude of the scattered intensity can be primarily explained by the increase in the volume fraction of the consolidating sample with time. The small differences in the values can be attributed to the different settling geometries and volume fraction variations

TABLE I. The table provides values for ϕ_f/ϕ_0 from settling measurements and $[I_{sc}(q)]_f/[I_{sc}(q)]_0$ from scattering measurements for samples at $\phi=0.08$ and various polymer concentrations.

c/c^*	ϕ_f	ϕ_f/ϕ_0	$[I_{sc}(q)]_f/[I_{sc}(q)]_0$
0.25	0.24	3	4.3±0.5
0.4	0.215	2.7	3.7±0.5
0.5	0.2	2.5	1.9±0.2
0.6	0.176	2.2	2.4±0.3
0.8	0.12	1.5	1.1±0.2

within the bed. The ability to superimpose the scattering intensities from the sediment at different times with a single shift factor and the observation that this shift factor is directly related to an independent measure of the average volume fraction in the sediment suggests that $S(q)$ for a given suspension is constant over the window of accessible wave vectors as its volume fraction increases with settling at a constant polymer concentration.

The structure factors from suspensions immediately after loading is given in Fig. 4(a) plots for samples at $\phi=0.08$ and different polymer concentrations. For the entire range of polymer concentrations at $\phi=0.08$, we see an overlap of $S(q)$ for all values of q [an expanded view is shown in the inset of Fig. 4(a)]. As discussed earlier with the absolute intensities in Fig. 3(a), there exists a prominent first peak in the static structure factor, $S(2q^*R)$ at $2q^*R\sim7.4$. Except for the sample, $c/c^*=0.25$, which has a slightly higher value of ~2.8, the value of $S(2q^*R)\sim2$ for the remaining polymer concentrations. The large values of $S(2q^*R)$ obtained at a volume fraction of 0.08 indicate that particles have highly correlated positions while the absolute value of $2q^*R$ indicates that the particles are localized in positions where they are essentially at contact. The contact value for the depletion attraction can be estimated from the Asakura-Oosawa (AO) model [34] as $u(2R)=\frac{3}{2}\frac{R}{Rg}\frac{c}{c^*}k_BT$ indicating that at the fluid-fluid-cluster phase boundary $u(2R)\sim2k_BT$ while at $c/c^*=0.8$, $u(2R)\sim15k_BT$. This suggests that clusters form when attractions exceed a few times the average thermal energy in the system ($\sim2-3k_BT$) while the cluster microstructure as characterized by the center of mass correlations and the spacing between the particles is a very weak function of the strength of attraction.

In the low wave-vector region ($2qR<1$), there is a strong upturn in the structure factor which is similar to that reported in space-spanning depletion gels on similar experimental systems [28,29,35] at high volume fractions of $\phi=0.20-0.40$. This low-angle upturn has also been observed in the scattering profiles of a number of different systems [36–41]. In fractal interpretations of scattering from gels and aggregated systems, a power-law dependence of scattering on the wave vector is taken as an indication of fractal behavior. In dense suspensions, the ability of clusters to be fractals must be discounted and the low q behavior instead has been interpreted as originating from randomly distributed heterogeneities within the gel. The correlation length between these heterogeneities, deduced by the Debye-Bueche treatment [30] involving scattering from a "random two-phase" model, was on the order of 5–8 times the particle diameter [29,35]. We note that the negative power law slopes at low q in the insets of Figs. 4(a)–4(c) have values of 3–4 indicating again that for these systems a fractal origin of the scattering at these wave vectors cannot capture the observed behavior even at volume fractions of 0.08. Additionally, since their slopes approach a value of −4, the scattering can be attributed to resulting from objects with sharp interfaces. Therefore, we again interpret the scattering as originating from dense clusters with the upturn at low q arising from the distribution of heterogeneities within these clusters.

For scattering from spherical clusters at low volume fractions ($\phi<0.10$), one expects a roll-off from the low-angle Guinier plateau at a normalized wave vector of $qR_c\sim1$ where R_c is the radius of the cluster. The absence of a plateau in the $S(q)$ at the lowest accessible wave vectors in our USAXS experiments ($q_{\min}\sim0.001$ nm^{-1}) suggests that the radii of the particle clusters, R_c, settling are larger than $(20-25)R$. Hence we conclude from Fig. 4(a) that above a critical polymer concentration, particles aggregate into clusters with sizes much larger than $(20-25)R$ and with internal microstructures similar to those observed for space spanning depletion gels at much higher volume fractions on similar length scales.

Figure 4(b) plots $S(2qR)$ as a function of $2qR$ as it evolves with time for the sample, $\phi=0.08$ and $c/c^*=0.6$. For these calculations, in order to determine the sediment ϕ for a scattering run at any time, we have employed the equation, $\phi=\phi_0(I_{sc}(q)/[I_{sc}(q)]_0)$, where as pointed out in Table I, $(I_{sc}(q)/[I_{sc}(q)]_0)$ matches the ratio (ϕ/ϕ_0). As seen in the figure, $S(2qR)$ over the entire range of accessible wave vectors collapses on to a single curve for scattering runs at all times as expected from the analysis of Fig. 3(b). This collapse is seen for all polymer concentrations investigated in this study. The appearance of a frozen microstructure indicates that as the particle clusters settle, their internal structure remains unchanged even as the final stages of the settling are reached where the sedimented cake forms a space-spanning network. Using a distinct colloidal system with depletion attractions but under similar conditions of ϕ, R_g/R and c/c^*, Lu *et al.* [13] also show that their cluster morphologies are independent of the colloid volume fraction.

As the volume fraction is increased from $\phi=0.08$ to 0.25 at fixed c/c^*, we again see no change in the microstructure over the accessible wave vectors [Fig. 4(c)]. For the data shown, the scattering was taken on homogeneous suspensions immediately after loading into the scattering cell. Of significance is that no settling is observed over a 10 hour period for $\phi=0.25$ and $c/c^*=0.40$ indicating that the sample is a space spanning gel that can support its weight. These results again support the conclusion that on length scales of $\sim20-25$ particle radii (corresponding to $\sim1/q_{\min}$) and smaller, the structures of the depletion gels and clusters in the fluid-cluster phase are nearly identical.

IV. DEBYE-BUECHE ANALYSIS

The studies of Shah *et al.* [29] over a range of R_g/R ratios and Ramakrishnan *et al.* [28] over a wide range of volume

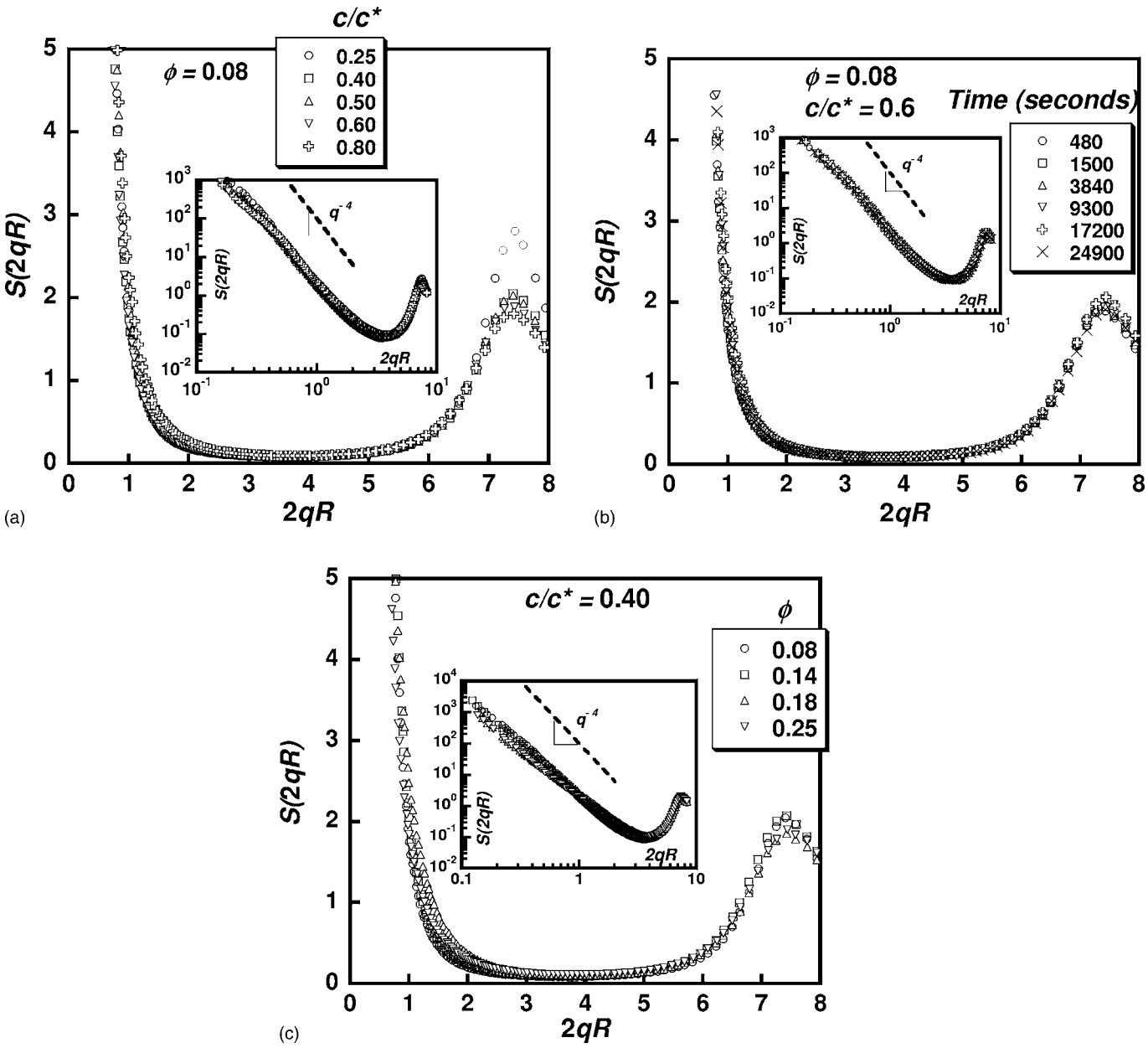

FIG. 4. (a) Static structure factor, $S(2qR)$, as a function of normalized wave vector, $2qR$, for all explored polymer concentrations at ϕ=0.08. A distinct first peak is observed at a $2q^*R \sim 7.4$. The magnitude of the first peak is ~2, except for c/c^*=0.25 for which it is ~2.8. This indicates strong correlations in density fluctuations on length scales of a particle diameter. The low angle upturn is similar to that observed in depletion gels at much higher volume fractions of $\phi \sim 0.40$. The inset plot shows that $S(2qR)$ is nearly identical for all polymer concentrations over two orders in magnitude of the scattering wave vector, $2qR$. The dotted line in the inset is a reference line with a power law slope of −4. (b) $S(2qR)$ as a function of the normalized wave vector, $2qR$, for ϕ=0.08 and c/c^*=0.6. The structure remains frozen as the local volume fraction increases due to the settling of the sample. Over the entire range of accessible wave vectors, there is no change in $S(2qR)$ as seen in the inset. This evidence of a frozen microstructure is observed for all the samples in our study. The dotted line in the inset is a reference line with a power law slope of −4. (c) $S(2qR)$ as a function of the normalized wave vector, $2qR$, for samples at a polymer concentration of c/c^*=0.40 and increasing volume fraction. The data shown are for runs performed immediately after loading the suspension into the USAXS sample cell. The inset figure shows the same data expanded on a log-log scale. The dotted line in the inset is a reference line with a power law slope of −4.

fractions (ϕ=0.20–0.40) explored the microstructure of space-spanning depletion gels using a similar experimental system with USAXS techniques. To understand the Porod-like scattering that resulted in the low angle upturns in their $S(q)$, similar to different materials [39–41], they hypothesized that the strong scattering at low qR results from voids that are randomly distributed within the network of the gel. They used a "random two-phase" model proposed by Debye and Bueche [30] to explain scattering from randomly distributed quenched heterogeneities by defining a heterogeneity

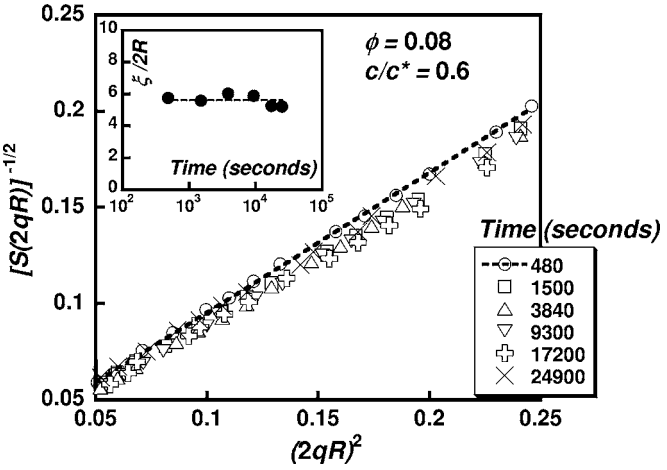

FIG. 5. $[S(2qR)]^{-1/2}$ against $(2qR)^2$ at low $2qR$. According to the Debye-Bueche analysis [30] for scattering from randomly scattered heterogeneities, the intercept and the slope of the linear fit provide information on the characteristic length scale, ξ, for the distribution of these heterogeneities. The inset shows how $\xi/(2R)$ remains unchanged as the sample settles with time.

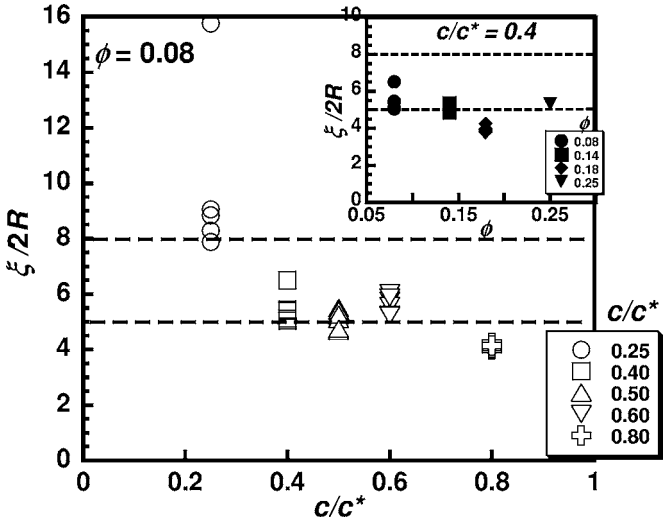

FIG. 6. $\xi/(2R)$ as a function of polymer concentration, c/c^*. Multiple points at each c/c^* are values obtained from scattering runs at different times after loading the sample. The figure shows that $\xi/(2R)$ remains relatively insensitive to polymer concentration except at $c/c^*=0.25$ which is obtained from the initial run. The upper and lower dotted lines are the limits for $\xi/(2R)$ obtained for space-spanning depletion gels [29,35]. In the inset plot, $\xi/(2R)$ is plotted as a function of colloid volume fraction at constant polymer concentration. The dotted lines have the same meaning as in the main figure.

distribution function in real space as $\langle \eta^2 \rangle \exp(-r/\xi)$ where $\langle \eta^2 \rangle = \langle (\delta\rho)^2 \rangle / \rho^2$ is a dimensionless mean square number density difference between the gel network and the voids and ξ is the characteristic distance between heterogeneities. In Fourier space, the Debye-Bueche scattering function is defined as

$$S_{\mathrm{DB}}(q) = \frac{S_{\mathrm{DB}}(0)}{(1+q^2\xi^2)^2},$$

$$S_{\mathrm{DB}}(0) = 48\phi\left(\frac{\xi}{2r}\right)^3 \langle \eta^2 \rangle, \tag{1}$$

and the total structure factor is given by $S(q)=S_{\mathrm{DB}}(q)+S_{\mathrm{reg}}(q)$. Here $S_{\mathrm{reg}}(q)$ represents the scattering from smaller length scale fluctuations of equilibrium or near-equilibrium origin. Assuming the Debye-Bueche contributions dominate the scattering at wave vectors where we see the low angle upturn, a linear fit to the plot of $S(2qR)^{-1/2}$ against $(qR)^2$ provides an intercept that gives $S_{\mathrm{DB}}(0)$ and a slope that gives us information about $(\xi/2R)$. As seen in Fig. 5, over the low wave-vector scattering region, when plotted in this manner, our data for the sample, $\phi=0.08$ and $c/c^*=0.6$ at various settling times yields a linear plot from which we can extract a time independent intercept and slope. Similar curves are obtained for all samples employed in this study yielding $S_{\mathrm{DB}}(0) \sim 4\times10^2 - 1\times10^4$ for these samples. The significantly higher values in our study, obtained primarily at the low volume fraction of $\phi=0.08$ and $c/c^*=0.25-0.6$, in comparison with values of $\sim 3\times10^2 - 8\times10^2$ obtained in the dense depletion gels of Shah *et al.*[29] indicate stronger fluctuations between the mean densities in the dense clusters and the distributed voids. This is consistent with the observations of Ramakrishnan *et al.* [35] where they report a similar increase in the difference between the number densities in the dense clusters and voids with a decrease in the particle volume fraction. The inset plot of Fig. 5 shows that over time as the clusters settle, values for $(\xi/2R)$ remain nearly constant at $\sim 5-6$.

Values of the normalized correlation length, $(\xi/2R)$ at $\phi=0.08$ for all polymer concentrations explored in the study are shown in Fig. 6. The multiple points at a single polymer concentration represent values obtained from scattering runs performed at different times. For the sample, $\phi=0.08$ and $c/c^*=0.25$, we obtain $(\xi/2R)=15.75$ during the initial run, a value substantially higher than what we extract for all other samples, a trend qualitatively similar to the behavior of $S(2q^*R)$ as well [Fig. 4(a)]. As time progresses and the clusters settle, the values for $(\xi/2R)$ and $S(2q^*R)$ decrease to what is extracted for the other samples. This suggests that at low volume fractions and under conditions of weak attractions, particles are more highly correlated and voids are more widely distributed than at later times, a behavior absent as we move deeper into the fluid-cluster phase. For all other samples, values for $(\xi/2R)$ fall in the range of $\sim 5-8$ which are identical to the values obtained by Shah *et al.* [29] and Ramakrishnan *et al.* [35] for space-spanning depletion gels. The inset of Fig. 6 shows the characteristic length, $(\xi/2R)$, as a function of constant polymer concentration, $c/c^*=0.40$ and different volume fractions. Again, the characteristic length scale for the distribution of voids within the particle cluster is within the window of $\sim 5-8$ obtained in previous studies [29,35]. The similarities in the characteristic length scale for the distribution of heterogeneities within the clusters in the fluid-cluster phase and the space-spanning depletion gels suggest that for the range of R_g/R, c/c^* and ϕ explored in these systems, depletion gels are composed of clusters that

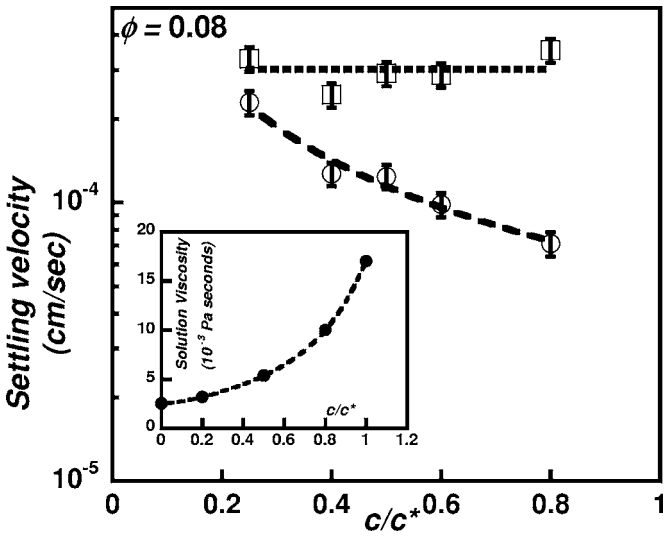

FIG. 7. Initial settling velocity as a function of the polymer concentration. The lines through all data are drawn to guide the eye. The open circles are settling velocities extracted from a linear fit to the initial settling profiles. The open squares are settling velocities obtained after correcting for the medium viscosity change due to the presence of the polymer. The inset displays the dependence of medium viscosity on polymer concentration with the line through the data representing a fourth degree polynomial fit. As seen in the main figure, the corrected settling velocities are independent of polymer concentration. This suggests that to a first-order approximation, the sizes of the settling clusters are independent of polymer concentration.

have percolated to form a space-spanning network. What sets the characteristic size for cluster formation remains an open question.

V. DISCUSSION

To get an estimate of how the average cluster size depends on the polymer concentration, we revert to the initial settling velocities from the settling experiments. In Fig. 7 we replot the settling velocities as a function of polymer concentration at $\phi=0.08$. At first glance, the decrease in settling velocity, u_{set}, suggests that the average cluster size decreases with increasing polymer concentration. However, changes in the viscosity of the continuous phase due to the presence of the polymer must be accounted for prior to making any conclusions. The continuous phase viscosity in the presence of the polymer, η_{poly}, is shown in the inset plot of Fig. 7. This reveals that the medium viscosities at the polymer concentrations employed in the study are substantially higher than the pure solvent viscosity, η_0. Correcting for this by multiplying the factor of increase, $(\eta_{\mathrm{poly}}/\eta_0)$ with u_{set} gives the actual settling velocity, $\bar{u}_{\mathrm{set}}$ of the clusters as shown by the open squares in the main plot. $\bar{u}_{\mathrm{set}}\sim 3\times 10^{-4}$ cm/s and independent of the polymer concentration suggesting that the particle clusters sizes are independent of polymer concentration if we assume a single size for these clusters. If we assume the settling to be in the Stokes-Einstein limit, then the cluster hydrodynamic radius can be determined from $R_c=\sqrt{\frac{9\bar{u}_{\mathrm{set}}\eta_0}{2\Delta\rho g}}$ where $\Delta\rho=900$ kg/m^3 and $g=9.8$ m/s^2 is the gravitational acceleration. Using the values for $\bar{u}_{\mathrm{set}}$ and η_0 mentioned above gives $R_c\sim 2\times 10^3$ nm or $\sim 50R$. Since the clusters are expected to have a structure that is porous to the solvent, as seen from the Debye-Bueche analysis, thereby enhancing its hydrodynamic resistance, the size estimate from the calculations is a lower bound.

X-ray scattering from suspensions of spherical clusters are expected to display a low angle (wave vector) Guinier plateau at a normalized wave vector, $qR_c\leq 1$. Since the lowest wave vector accessed in this study is $q_{\mathrm{min}}\sim 0.001$ nm^{-1} and the lowest estimate of the cluster size is $\sim 2\times 10^3$ nm, therefore $q_{\mathrm{min}}R_c\geq 2$ in our study. Thus the cluster size estimate from the settling velocity agrees with the observation that we are unable to access the low angle Guinier plateau for the clusters from our USAXS experiments. In addition, this also confirms that the USAXS experiments are probing the microstructure on length scales smaller than that of the average cluster sizes and therefore within the cluster.

Scattering studies and first-order estimates of the cluster sizes from our experiments shed light on the internal microstructure of these particle clusters. However, the fundamental cause for the presence of a fluid-cluster phase as a precursor to colloidal gelation remains unanswered.

VI. CONCLUSION

A number of studies [4,12–14] report the formation of an "equilibrium" phase consisting of clusters of particles in depletion systems where the polymer concentration is increased above a volume fraction dependent value. These phases have been observed with experimental systems composed of sterically stabilized poly(methyl methacrylate) (PMMA) particles when $R_g/R\sim 0.1$ or lower and in the octadecyl-coated silica particle system studied here when $R_g/R<0.1$. As the polymer concentration or volume fraction is increased, these clusters ultimately form a space filling gel. Segre *et al.* [14] proposed that the colloidal gel phase was essentially driven by a glasslike transition at a critical volume fraction where fluid clusters achieved a "jammed" state thereby percolating to form a gel. This would indicate that on length scales smaller than the characteristic size of a particle cluster, one would see no distinction in the microstructure within the gel or the equilibrium cluster phase. Indeed, our observations from scattering experiments where we increase the sample volume fraction at a constant polymer concentration, $c/c^*=0.40$, concurs with this hypothesis.

However cluster size estimates from our settling experiments at a constant volume fraction of $\phi=0.08$ and increasing polymer concentrations, $c/c^*=0.25-0.80$ show that cluster sizes to a first approximation are independent of polymer concentration. This suggests that if the clusters are not growing larger with increasing polymer concentration and their number density is constant, jamming alone cannot explain a transition into the gel phase. On the other hand, it seems more likely that the stronger attractions eventually force the clusters to percolate and form space-spanning gels. Thus attractions must have a role to play in addition to crowding effects in determining the boundary between fluid-cluster

and gel phases for depletion gels. Outstanding questions revolve around the system-dependent physics that sets the cluster size and the physics that ultimately drives the kinetic arrest of particles in clusters and the subsequent percolation of these clusters, above the boundary between fluid-cluster and gel phases, to form space-spanning gels.

ACKNOWLEDGMENTS

The authors acknowledge Professor Ramakrishnan for the experimental data on the gel boundaries. The authors thank J. Ilavsky for support in gathering USAXS data at the synchrotron facility at the Argonne National Laboratory. Use of the Advanced Photon Source was supported by the U. S. Department of Energy, Office of Science, Office of Basic Energy Sciences, under Contract No. W-31-109-ENG-38. SEM measurements for this paper were carried out in the Center for Microanalysis of Materials, University of Illinois at Urbana-Champaign, which is partially supported by the U. S. Department of Energy under Grant No. DEFG02-91-ER45439. This work was supported by the Nanoscale Science and Engineering Initiative of the National Science Foundation under NSF Grant No. DMR-0117792.

[1] S. A. Shah *et al.*, J. Chem. Phys. **118**, 3350 (2003).
[2] S. Ramakrishnan *et al.*, J. Chem. Phys. **116**, 2201 (2002).
[3] C. J. Rueb and C. F. Zukoski, J. Rheol. **41**, 197 (1997).
[4] W. C. K. Poon, A. D. Pine, and P. N. Pusey, Faraday Discuss. **101**, 65 (1995).
[5] M. C. Grant and W. B. Russel, Phys. Rev. E **47**, 2606 (1993).
[6] M. Chen and W. B. Russel, J. Colloid Interface Sci. **141**, 564 (1991).
[7] J. W. Jansen, C. G. Dekruif, and A. Vrij, J. Colloid Interface Sci. **114**, 481 (1986).
[8] D. A. Weitz *et al.*, Phys. Rev. Lett. **54**, 1416 (1985).
[9] P. Meakin, Phys. Rev. Lett. **51**, 1119 (1983).
[10] M. Y. Lin *et al.*, Nature (London) **339**, 360 (1989).
[11] M. Kolb, R. Botet, and R. Jullien, Phys. Rev. Lett. **51**, 1123 (1983).
[12] A. I. Campbell *et al.*, Phys. Rev. Lett. **94**, 208301 (2005).
[13] P. J. Lu *et al.*, Phys. Rev. Lett. **96**, 028306 (2006).
[14] P. N. Segre *et al.*, Phys. Rev. Lett. **86**, 6042 (2001).
[15] G. H. Bogush and C. F. Zukoski, J. Colloid Interface Sci. **142**, 19 (1991).
[16] V. Privman *et al.*, J. Colloid Interface Sci. **213**, 36 (1999).
[17] D. L. Van Hyning, W. G. Klemperer, and C. F. Zukoski, Langmuir **17**, 3128 (2001).
[18] W. C. K. Poon *et al.*, Faraday Discuss. **112**, 143 (1999).
[19] Y. L. Chen and K. S. Schweizer, J. Chem. Phys. **120**, 7212 (2004).
[20] J. Bergenholtz and M. Fuchs, Phys. Rev. E **59**, 5706 (1999).
[21] J. Bergenholtz, M. Fuchs, and T. Voigtmann, J. Phys.: Condens. Matter **12**, 6575 (2000).
[22] K. Dawson *et al.*, Phys. Rev. E **63**, 011401 (2001).
[23] L. Fabbian *et al.*, Phys. Rev. E **59**, R1347 (1999).
[24] J. Groenewold and W. K. Kegel, J. Phys. Chem. B **105**, 11702 (2001).
[25] R. Sanchez and P. Bartlett, J. Phys.: Condens. Matter **17**, S3551 (2005).
[26] A. Stradner *et al.*, Nature (London) **432**, 492 (2004).
[27] A. Yethiraj and A. van Blaaderen, Nature (London) **421**, 513 (2003).
[28] S. Ramakrishnan, V. Gopalakrishnan, and C. F. Zukoski, Langmuir **21**, 9917 (2005).
[29] S. A. Shah *et al.*, J. Phys.: Condens. Matter **15**, 4751 (2003).
[30] P. Debye and A. M. Bueche, J. Appl. Phys. **20**, 518 (1949).
[31] W. Stober, A. Fink, and E. Bohn, J. Colloid Interface Sci. **26**, 62 (1968).
[32] G. H. Bogush, M. A. Tracy, and C. F. Zukoski, J. Non-Cryst. Solids **104**, 95 (1988).
[33] A. K. Van Helden, J. W. Jansen, and A. Vrij, J. Colloid Interface Sci. **81**, 354 (1981).
[34] S. Asakura and F. Oosawa, J. Polym. Sci. **33**, 183 (1958).
[35] S. Ramakrishnan *et al.*, Phys. Rev. E **70**, 040401 (2004).
[36] M. A. Crichton and S. R. Bhatia, Langmuir **21**, 10028 (2005).
[37] S. R. Bhatia, Curr. Opin. Colloid Interface Sci. **9**, 404 (2005).
[38] D. Pontoni and T. Narayanan, J. Appl. Crystallogr. **36**, 787 (2003).
[39] M. S. Kalhoro *et al.*, Polymer **42**, 1679 (2001).
[40] D. Q. Wu *et al.*, Macromolecules **26**, 1000 (1993).
[41] J. M. Zhou and J. Sheng, Polymer **38**, 3727 (1997).